International Journal of Pharmaceutics 509 (2016) 208–218

Contents lists available at ScienceDirect

International Journal of Pharmaceutics

journal homepage: www.elsevier.com/locate/ijpharm

Biocompatible Zr-based nanoscale MOFs coated with modified poly (ε-caprolactone) as anticancer drug carriers

Maria Filippousi[a,*], Stuart Turner[a], Karen Leus[b], Panoraia I. Siafaka[c], Eirini D. Tseligka[d], Matthias Vandichel[e], Stavroula G. Nanaki[c], Ioannis S. Vizirianakis[d,f], Dimitrios N. Bikiaris[c], Pascal Van Der Voort[b], Gustaaf Van Tendeloo[a]

[a] EMAT, University of Antwerp, Groenenborgerlaan 171, B-2020 Antwerp, Belgium
[b] Department of Inorganic and Physical Chemistry, Center for Ordered Materials, Organometallics and Catalysis (COMOC), Ghent University, Krijgslaan 281-S3, 9000 Ghent, Belgium
[c] Laboratory of Polymer Chemistry and Technology, Aristotle University of Thessaloniki, GR-54124 Thessaloniki, Macedonia, Greece
[d] Laboratory of Pharmacology, School of Pharmacy, Aristotle University of Thessaloniki, GR-54124 Thessaloniki, Macedonia, Greece
[e] Center for Molecular Modeling, Universiteit Gent, Technologiepark 903, 9052 Zwijnaarde, Belgium
[f] Department of Life and Health Sciences, University of Nicosia, 1700 Nicosia, Cyprus

ARTICLE INFO

Article history:
Received 15 April 2016
Received in revised form 22 May 2016
Accepted 25 May 2016
Available online 26 May 2016

Keywords:
Metal-organic frameworks/UiO-66
UiO-67
Polymer
Drug delivery
SEM
ADF-STEM

ABSTRACT

Nanoscale Zr-based metal organic frameworks (MOFs) UiO-66 and UiO-67 were studied as potential anticancer drug delivery vehicles. Two model drugs were used, hydrophobic paclitaxel and hydrophilic cisplatin, and were adsorbed onto/into the nano MOFs (NMOFs). The drug loaded MOFs were further encapsulated inside a modified poly(ε-caprolactone) with D-α-tocopheryl polyethylene glycol succinate polymeric matrix, in the form of microparticles, in order to prepare sustained release formulations and to reduce the drug toxicity. The drugs physical state and release rate was studied at 37 °C using Simulated Body Fluid. It was found that the drug release depends on the interaction between the MOFs and the drugs while the controlled release rates can be attributed to the microencapsulated formulations. The *in vitro* antitumor activity was assessed using HSC-3 (human oral squamous carcinoma; head and neck) and U-87 MG (human glioblastoma grade IV; astrocytoma) cancer cells. Cytotoxicity studies for both cell lines showed that the polymer coated, drug loaded MOFs exhibited better anticancer activity compared to free paclitaxel and cisplatin solutions at different concentrations.

1. Introduction

Oral chemotherapy is a long-term desirable alternative option for cancer therapeutics since it is less stressful for the patient and thus improves the quality of life of patients (Mei et al., 2013). Unfortunately, most anticancer drugs, especially those with high therapeutic efficacy such as taxanes (paclitaxel), vinca alkaloids, and noscapinoids, are not orally bioavailable (Jiang et al., 2013). Indeed, bioavailability is considered a major success task within the new pharmaceuticals development era; drugs with poor bioavailability fail to reach the minimum effective concentration, which is required to achieve the expected pharmacological treatment outcome (Jain et al., 2013). Toxicity and biocompatibility are two important requirements related to the material considered as a potential drug carrier. In order to reduce the severe side effects and increase the therapeutic efficacy of water soluble drugs, the development of new non-toxic and biocompatible drug-delivery systems is needed.

Recently, a rapid growth in the field of porous materials as potential drug delivery systems has been reported (Filippousi et al., 2015; Horcajada et al., 2010; Trewyn et al., 2007; Zhuang et al., 2014). Metal organic frameworks can be regarded as potential drug carrier nanovehicles because of the ability to tune their pore size and the possibility to adjust the framework's functional groups (Horcajada et al., 2008; Huxford et al., 2010; Keskin and Kızılel, 2011; Della Rocca et al., 2013). Because of these interesting material properties, new approaches have been developed to synthesize MOFs that are scaled-down to the nanoregime (Meledina et al., 2016; Taylor-Pashow et al., 2009). Férey (2008) were the first to report the use of MOFs and specifically the MIL-n family (MIL = Materials of Institut Lavoisier) as potential drug carriers (Férey, 2008). Zhu et al. (2014) have more recently

* Corresponding author.
E-mail address: maria.filippousi@ua.ac.be (M. Filippousi).

http://dx.doi.org/10.1016/j.ijpharm.2016.05.048
0378-5173/

Table 1
List of the samples together with their abbreviations.

S1: UiO-66	S8:UiO-66 loaded with cisplatin
S2: UiO-67	S9: UiO-67 loaded with cisplatin
S3: PCL-TPGS	S10: UiO-66 loaded with taxol and encapsulated in PCL-TPGS
S4: taxol	S11: UiO-67 loaded with taxol and encapsulated in PCL-TPGS
S5: cisplatin	S12: UiO-66 loaded with cisplatin and encapsulated in PCL-TPGS
S6:UiO-66 loaded with taxol	S13: UiO-67 loaded with cisplatin and encapsulated in PCL-TPGS
S7: UiO-67 loaded with taxol	

employed the Zr-based MOFs (UiO-66) as anticancer drug delivery vehicles. However, MOFs are usually unstable in an aqueous solution, forming large aggregates, which might lead to unwanted side effects.

Microparticulate systems using synthetic biodegradable polyester polymers are widely used for controlled drug release and biomedical applications. Such materials consist of either synthetic or natural polymers which can easily be degraded in vivo by alternative ways (enzymatically or not). The latter process produces biocompatible or nontoxic products along with the progressive release of dissolved-dispersed drug (Filippousi et al., 2013a, 2013b). Poly(ε-caprolactone) (PCL) is utilized in such applications because of its biocompatibility and non-toxicity. Its carbonyl groups are steadily functionalized with various hydrophilic segments, such as poly(ethylene glycol) (PEG) in order to overcome and avoid the reticuloendothelial system, creating long-circulating "stealth" nano-carriers (Sinha and Trehan, 2003). D-α-Tocopheryl polyethylene glycol 1000 succinate (TPGS) is a water-soluble derivative of natural vitamin E (VitE) and polyethylene glycol (PEG) 1000. TPGS is a safe and effective form of VitE (Sokol et al., 1993) for reversing or preventing VitE deficiency, because of its good per os bioavailability. Additionally it has been reported to increase the oral bioavailability of anticancer drugs.

In this work a poly(ε-caprolactone)–tocopheryl polyethylene-glycol-succinate (PCL–TPGS) copolymer was synthesized to engineer the surface of two Zr-based NMOFs, UiO-66 and UiO-67, to improve drug solubility and generate an optimal drug delivery carrier. The drug loading efficiency and drug release properties of the polymer-drug loaded NMOFs were investigated using two model drugs: hydrophilic cisplatin and hydrophobic taxol. TPGS-block-PCL copolymers were synthesized (Ren et al., 2009) and characterized by proton nuclear magnetic resonance (^{1}H NMR) and fourier transform infrared spectroscopy (FTIR). Microparticles of TPGS-block-PCL copolymer were produced using a solid-oil-water technique(Marquette et al., 2014) and studied using scanning electron microscopy (SEM) and annular dark field scanning transmission electron microscopy (ADF-STEM). *In vitro* release studies were performed in a Dissolution Distek Apparatus (Evolution 4300) using simulated body fluids at 37 °C. Since drug release characteristics depend on the hydrophilicity of the drug, it

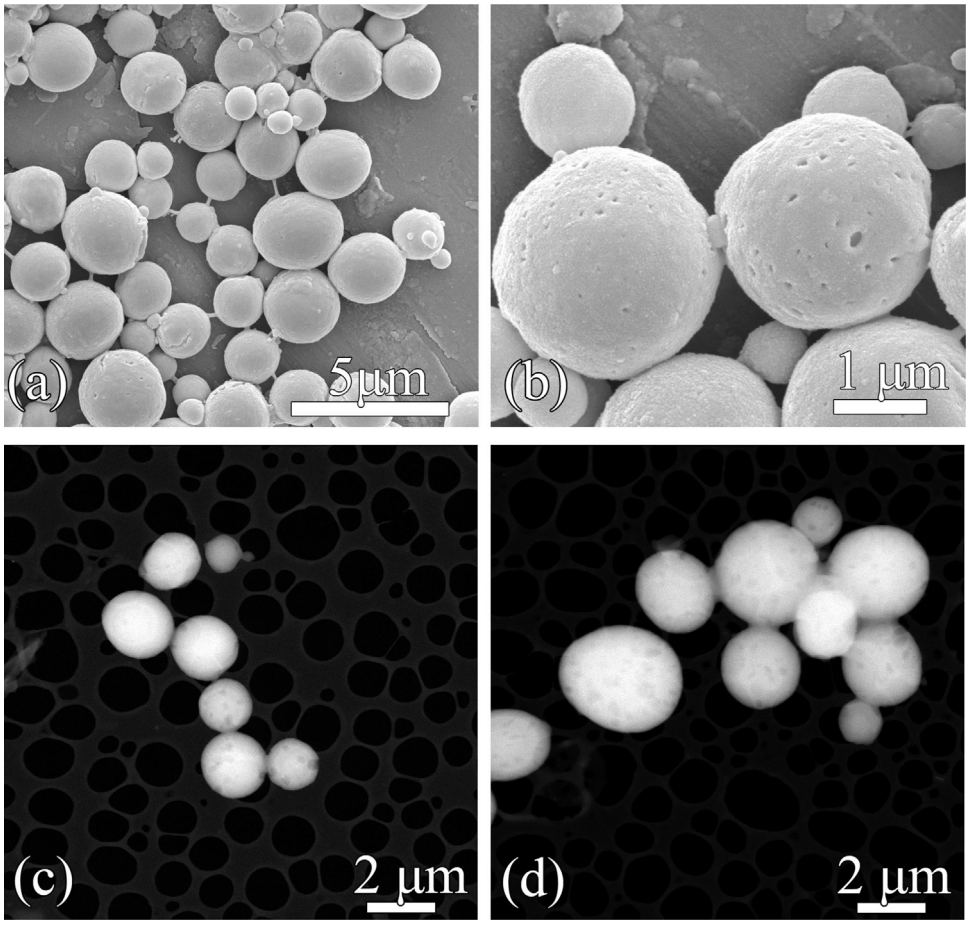

Fig. 1. (a) and (b) SEM images and (c) and (d) ADF-STEM images of the polymeric microparticles where pores in the surface can be observed.

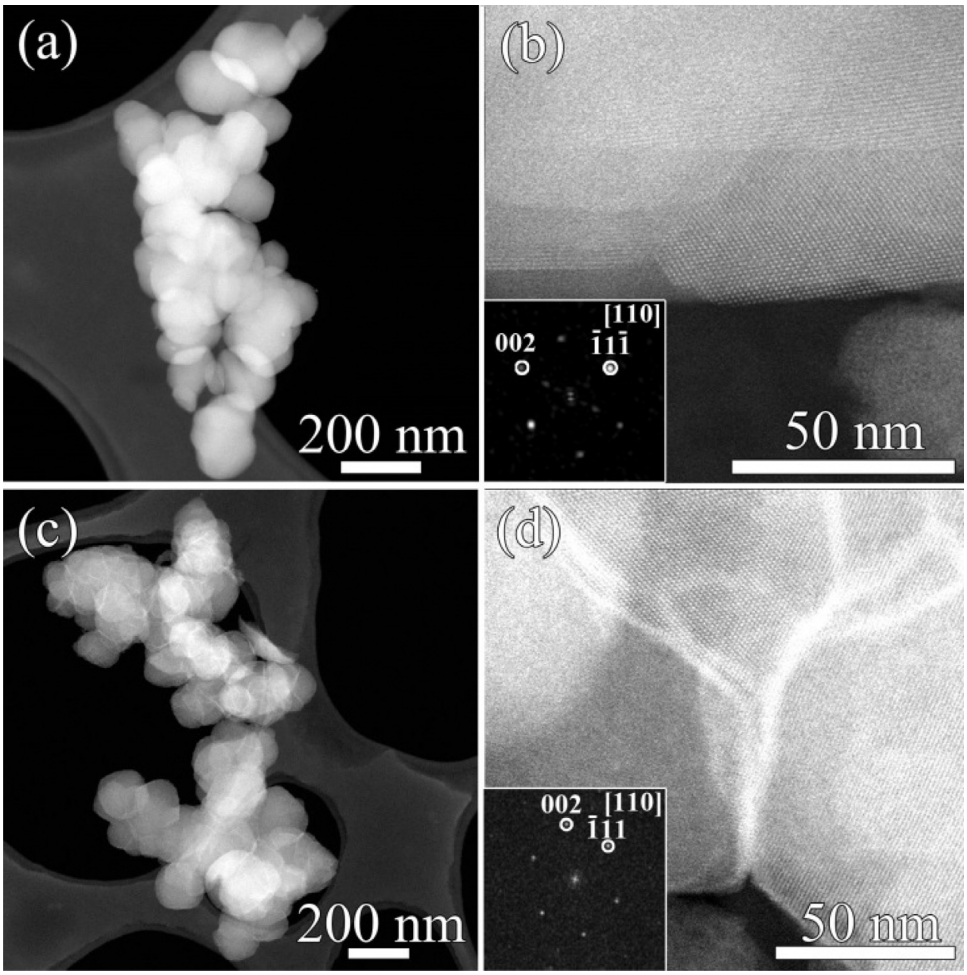

Fig. 2. Low and high magnification ADF-STEM images of the (a) and (b) UiO-66 sample and (c) and (d) UiO-67 sample. The insets illustrate the crystalline character.

was confirmed that the hydrophilic cisplatin was released at a much higher rate compared to the hydrophobic taxol. The *in vitro* cytotoxicity behavior of all the studied samples has been assessed against HSC-3 (human oral squamous carcinoma; head and neck) and U-87 MG (human glioblastoma grade IV; astrocytoma) cancer cells.

2. Results and discussion

In Table 1 a list of the materials that were used in the present work, together with their abbreviations is provided. In the rest of the manuscript we will refer to the samples, where needed, by their abbreviations.

2.1. Characterization of the polymers. Confirmation of the Co-polymerization with FTIR and ^{1}H NMR

In order to confirm the successful synthesis of PCL-block-TPGS copolymer FTIR and ^{1}H NMR studies were conducted (See in Supporting information Figs. S1 and S2). FTIR spectra of the neat PCL revealed the characteristic peaks of the polyester group which can be attributed to the carbonyl ester stretching C=O at 1733 cm^{-1}. These observations are in agreement with the work of Ciardelli et al. (2005) The asymmetric COC bond at 1240 cm^{-1} can also be observed. In the case of TPGS, the carbonyl acid group appears at 1730 cm^{-1}. However when TPGS is copolymerized with PCL, the carbonyl band is shifted to 1725 cm^{-1}. This shifting can be attributed to successful addition of TPGS into the PCL backbone. Additionally, a broad peak at 3466 cm^{-1} is observed due to the terminal hydroxyl group of TPGS. However, when the TPGS is copolymerized with the PCL the same peak is shifted to 3458 cm^{-1}. These shifts may reveal the successful copolymerization of PCL with TPGS. From ^{1}H NMR spectroscopy the alteration of the spectrum of PCL can be also confirmed when TPGS is added. The signals at 4.1 and 2.3 ppm were assigned to the methylene protons of PCL segment. The peaks at 4.07, 2.32, 1.61–1.71 and 1.34–1.44 were attributed to —OCH2, —COCH2, —CH2(4H) and —CH2(2H) segment of PCL, respectively (Ma et al., 2010). The strong peak at 3.6 ppm is assigned to the —CH2 protons of the PEG part of TPGS. Lower peaks can also be observed in the aliphatic region due to the existence of VitE (Ren et al., 2009).

2.2. Characterization of the PCL-TPGS by electron microscopy

The morphological characterization of the polymeric matrix and its ability to form microparticles was performed by SEM, ADF-STEM and XRPD (For the XRPD measurements see in Supporting information Fig. S3). Neat PCL-block-TPGS microspheres, prepared by an o/w emulsion method, have a spherical shape with an average diameter of 1–3 μm (Fig. 1). Both SEM and ADF-STEM images show that the surface of the PCL-TPGS microparticles has slight imperfections in the form of visible pores. Those pores might

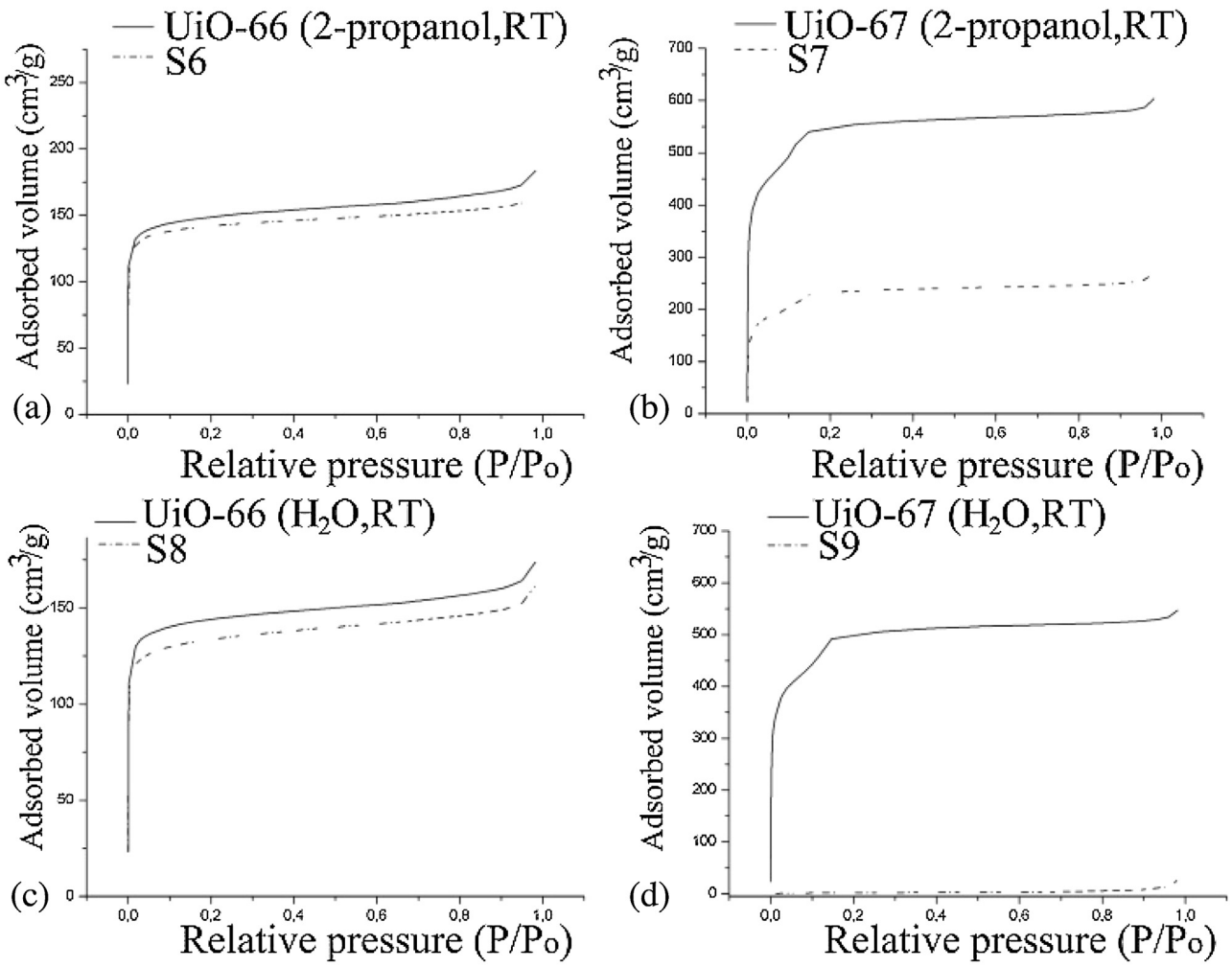

Fig. 3. Nitrogen adsorption isotherms of (a) UiO-66 (2-propanol, RT) and S6, (b) UiO-67 (2-propanol, RT) and S7 (c) UiO-66 (H2O, RT) and S8 and (d) UiO-67 (H2O, RT) and S9.

result from the water droplets which were trapped at the interior of the microspheres and evaporated during the drying process, leaving empty spaces. Similar results have been previously reported by Yang et al. (2001).

2.3. Characterization of the MOFs with electron microscopy

ADF-STEM and high resolution ADF-STEM measurements were carried out in order to study the structure, the size and the morphology of the nano MOFs. The unloaded UiO-66 and UiO-67 samples consist of well crystallized and faceted nanocrystals, which have the tendency to aggregate. Their dimensions range from 100 to 250 nm. In Figs. 2(b) and (d), high resolution ADF-STEM images of two different crystals are presented, oriented along the [110] zone axis, which allowed us to confirm, together with the XRPD measurements (Supporting information Fig. S4), the cubic structure of the nano MOFs (Zhu et al., 2013).

2.4. N2 adsorption measurements, elemental analysis

Fig. 3 shows the nitrogen adsorption isotherms of the UiO-66 and UiO-67 framework after stirring at RT for 24 h in the solvent (2-propanol or H2O) used during adsorption of the drug and after the actual adsorption of taxol or cisplatin. Additionally, in Table 2, the Langmuir surface area, pore volume and drug loading is presented of the pristine MOF materials, after stirring in H2O or 2-propanol

Table 2
Langmuir surface area, pore volume and drug loading of the pristine MOF materials, after stirring the materials in the solvent used during the adsorption and after loading with taxol or cisplatin.

	Langmuir surface area (m2/g)	Pore volume (cm3/g)	Cisplatin/taxol loading (mg/g)
UiO-66 pristine	840	0.32	–
UiO-67 pristine	2710	0.99	–
UiO-66 (2-propanol, RT)	712	0.28	–
UiO-67 (2-propanol, RT)	2530	0.93	–
UiO-66 (H2O, RT)	683	0.27	–
UiO-67 (H2O, RT)	2325	0.85	–
S6	672	0.25	140
S7	1114	0.41	100
S8	638	0.25	48
S9	13	~0	10

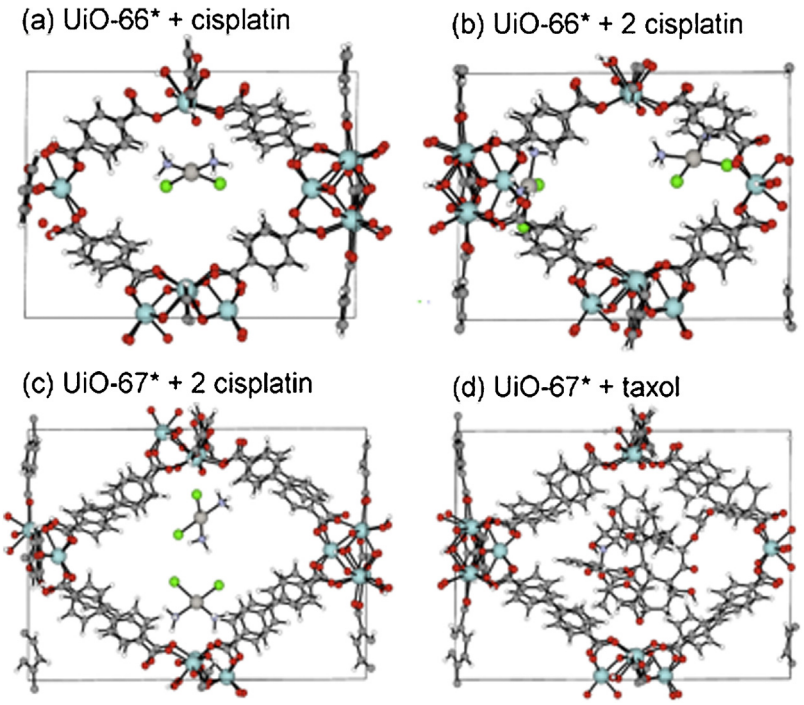

Fig. 4. Visualization of the MD-simulation after 5000 fs.

and after loading the drug. Table 2 indicates that there is only a minor decrease in the Langmuir surface area and pore volume of UiO-66 and UiO-67 after stirring both frameworks in 2-propanol and H2O in comparison to the pristine materials, showing that they are stable under the adsorption conditions.

Elemental analysis showed that 140 mg/g taxol is loaded onto the UiO-66 and 100 mg/g is loaded onto the UiO-67 framework, in spite of the higher surface area and larger pores of the latter. We therefore measured the nitrogen isotherms of the drug loaded UiO-66 and UiO-67 as well. The Langmuir surface area of the taxol loaded UiO-66 (S6) decreased only slightly in comparison to the UiO-66 (2-propanol, RT), from 712 m^2/g to 672 m^2/g. Also the pore volume decreased only marginally from 0.28 cm^3/g towards 0.25 cm^3/g. Taking into account the weight gain of the sample with 14% upon drug adsorption, the changes in surface area and pore volume are solely attributed to this weight gain and all taxol must be adsorbed on the outer surface of the UiO-66. This is to be expected as the size of the taxol is too large to enter the pores of the UiO-66 (vide infra). The taxol loaded UiO-67 framework (S7) on the other hand shows a significant decrease in the Langmuir surface area and pore volume in comparison to UiO-67 (2-propanol, RT). The Langmuir surface area decreases from 2530 m^2/g towards 1114 m^2/g and the pore volume decreases from 0.93 cm^3/g to 0.41 cm^3/g. These differences are much larger than the 10% weight gain and suggest that the taxol is probably adsorbed inside the pore system with partial pore blocking. XRPD patterns after drug adsorption show that the crystal structure of UiO-66 is unaffected by the adsorption. A similar conclusion can be drawn for taxol adsorption in UiO-67. However cisplatin seems to significantly affect the crystallinity of UiO-67, the main diffraction peak at 7° is still present, but higher order diffractions vanish. The peak at 7° corresponds to the (1,1,1)-plane containing the zirconia clusters. The peak broadening in this reflection and the disappearance of reflections at higher angles indicate the disappearance of long range order and a (at least partial) decomposition of the material. Note that for the cisplatin@UiO-66 (S8) again only a very slight decrease is noted in the Langmuir surface area and pore volume in comparison to UiO-66 (H2O, RT). Also, the loading of cisplatin on UiO-66 (48 mg/g) is rather low. This is also due to the hydrophilic nature of the cisplatin in comparison to the hydrophobic MOF linkers, explaining the higher loading of the hydrophobic taxol molecules. Although cisplatin could in principle enter the UiO-66 pore system, we have no exclusive evidence for this.

Surprisingly, the cisplatin@UiO-67 material (S9) has completely lost its porosity, although the loading of the cisplatin is only 10 mg/g. Although the UiO-67 is very stable in water (see the supporting information) and also relatively stable upon water stirring for 24 h (see Table 2; the pore volume only slightly reduces from 0.99 to 0.85 cm^3/g), we have to conclude here that the combined expose to water and cisplatin causes an amophisation of the UiO-67 structure. This is further illustrated in the XRPD patters in Fig. S4, where the cisplatin@UiO-67 shows broadened XRPD peaks. However, some crystallinity is maintained, as a partial pore filling/pore clogging cannot be excluded, as cisplatin easily fits the pore system of UiO-67.

2.5. Adsorption study of taxol and cisplatin within UiO-66 and UiO-67

To obtain more insight in the adsorption of taxol and cisplatin within UiO-66 and UiO-67, we first tried to incorporate the species within the model structure of UiO-66 and UiO-67 (Cavka et al., 2008). It is clear that adsorption of larger molecules such as taxol is not possible without the presence of defects. Basically there are two types of defects possible within these materials. The smaller defects arise via missing linkers within the Zr-MOFs (Vandichel et al., 2015), while the larger defects arise via missing inorganic Zr6O4(OH)4-bricks within these materials (Cliffe et al., 2014). Incorporation of more defects within UiO-type materials can be achieved by application of different synthesis procedures employing mono-carboxylate modulators (Cliffe et al., 2014; Vermoortele et al., 2013); a procedure that was first proposed by the Farrusseng group to increase the catalytic activity (Farrusseng et al., 2009;

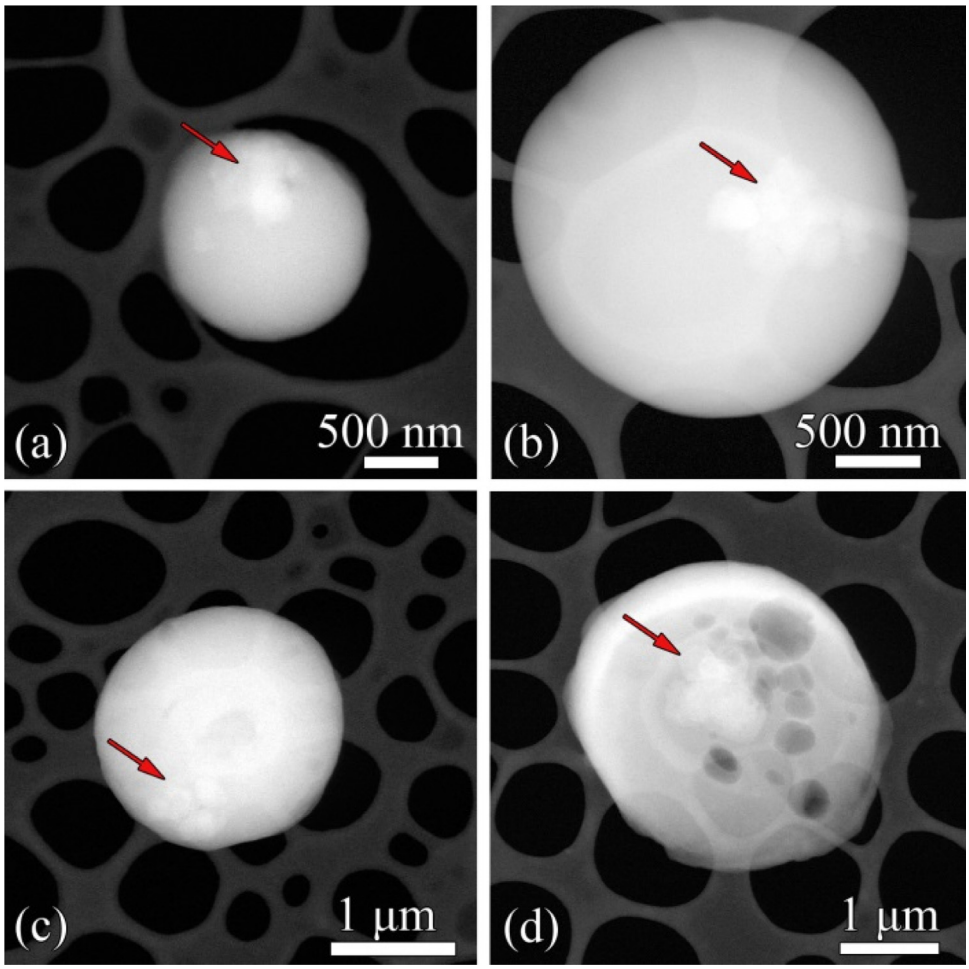

Fig. 5. ADF-STEM images of the polymer encapsulated drug loaded nano MOFs. PCL-TPGS encapsulated (a) UiO-66 loaded with taxol, (b) UiO-67 loaded with taxol, (c) UiO-66 loaded with cisplatin and (d) UiO-67 loaded with cisplatin in which a visibly porous PCL-TPGS polymeric matrix can be noticed. The red arrows indicate that the dug loaded MOF nanoparticles are located inside the co-polymer microspheres. (For interpretation of the references to colour in this figure legend, the reader is referred to the web version of this article.)

Ravon et al., 2010, 2008). The size of the adsorbate molecules determines which type of defect is at least required for incorporation within the framework.

Taxol cannot be incorporated within a UiO-66 model that has only linker defects; the incorporation of taxol clearly requires larger crystal defects, such as missing inorganic brick defects. Whenever such type of defects are present in large amounts (and with a certain periodicity), correlated defect nano regions (Cliffe et al., 2014) arise which create adsorption channels within the material, able to take up taxol (Fig. S5). Within UiO-67, linker defects generate already sufficient porosity to accommodate taxol molecules. Taxol fits just within a UiO-67 having one linker defect (a schematic representation of the pore formed by a single linker defect is given in Fig. S6). However, the linker defects should occur frequently enough to create diffusion channels for the taxol molecules. On the other hand, cisplatin is a much smaller molecule and can diffuse into UiO-67 without any problem. The smallest pores are still large enough to allow diffusion of cisplatin. Within UiO-66 however cisplatin can hardly diffuse through the small triangular windows, an event that was not observed during the MD-simulation of 50 ps. Fast diffusion of cisplatin within the UiO-66 materials therefore needs the presence of at least some linker defects.

For further insight into the framework-adsorbate interactions and to assign bands of the adsorbates in the experimental IR spectrum, first principle molecular dynamics calculations were performed on adsorbed cisplatin and taxol within periodic models of UiO-66 and UiO-67 containing one linker defect (Fig. S5), indicated as UiO-66* and UiO-67*. However, as the experimental systems contain defects, no fair comparison could be made with experimental IR-spectra and therefore these data can be found in Supporting Information. Molecular dynamics simulations give insight in the mobility and adsorption locations of the molecules within the structures. We rendered a graphic after 5000 fs of the performed MD-simulation to visualize the predominant adsorption positions of the adsorbate molecules (Fig. 4).

Cisplatin molecules are clearly interacting with the accessible basic site Zr-O-Zr of the inorganic bricks, which is the case for both UiO-66* and UiO-67* systems (Fig. 4a and c). In the UiO-67*, the void caused by the missing biphenyldicarboxylate linker makes it possible for two cisplatin molecules to interact with opposite Zr-O-Zr sites; in contrast to the UiO-66*, where only one of the two molecules did interact with a Zr-O-Zr site (Fig. 4b). In the experimental samples, the presence of solvent molecules will change the interactions with the Zr-O-Zr site and will lead to a further peak broadening of the IR-spectrum, which is exactly what

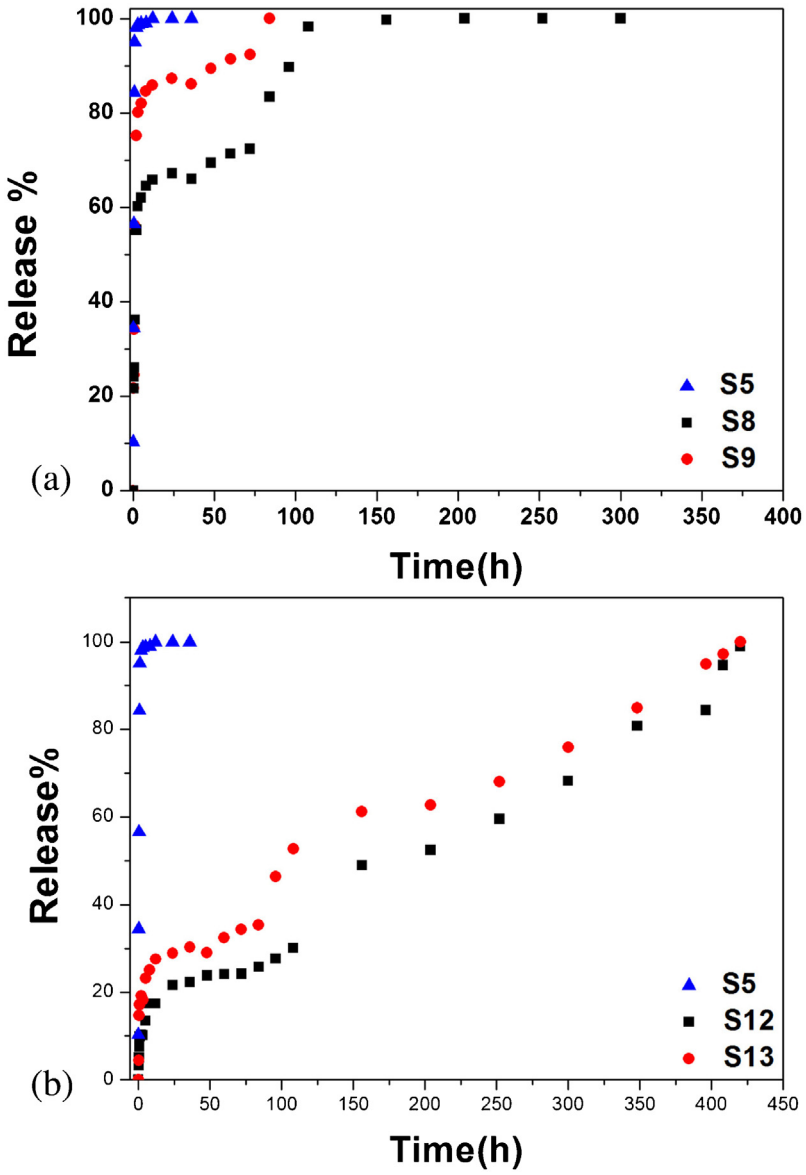

Fig. 6. Drug release pattern for (a) cisplatin and cisplatin loaded-MOFs and (b) polymer encapsulated cisplatin loaded forms.

we observe if we compare the velocity power spectra with the IR-measurements (see Supporting information).

From Fig. 4d, we see that taxol occupies the whole void that was created; throughout the entire MD-simulation the molecule occupied the middle of the created cage. Such limited mobility confirms that for taxol adsorption and diffusion within the pores of UiO-67, also inorganic brick defects required.

2.6. Characterization of the drug loaded MOFs and microencapsulated formulations into PCL-block-TPGS

2.6.1. XRPD

X-ray powder diffraction measurements were employed to investigate the structural evolution of the synthesized UiO-66 and UiO-67 loaded with the different drugs (See Fig. S4). The XRPD patterns of the pure drugs (taxol and cisplatin) show sharp diffraction peaks, indicating a clear crystalline structure (Mastropaolo et al., 1995; Milburn and Truter, 1966). By comparing the Bragg peaks of the drug loaded MOFs to those of the neat MOFs, it can be concluded that the drug loading did not modify the crystalline structure of UiO-66 (Horcajada et al., 2006). As no characteristic peaks of the crystalline drugs were recorded, the drug is loaded in amorphous form. PCL-block-TPGS is also a semicrystalline material with a degree of crystallinity of 55,7%. Moreover, a significant decrease of the relative peak intensity was observed for the drug loaded MOFs after encapsulation in the polymer, which could be ascribed to the higher concentration of the polymeric matrix. Additionally, the encapsulation of the polymeric matrix did not change the structure of the MOFs.

2.6.2. ADF-STEM for the polymer encapsulated drug loaded MOFs

The Zr-based NMOFs were used as drug loaded carriers and these materials were further microencapsulated into PCL-block-TPGS copolymer. Thus, in order to demonstrate the successful encapsulation of the drug loaded MOFs inside the polymeric microparticles, ADF-STEM measurements were performed. Fig. 5 illustrates the typical core-shell structure of the drug loaded MOFs embedded inside the polymeric microparticles (Zhao et al., 2014). In all cases, it could be confirmed that MOF nanoparticles are located inside the co-polymer microspheres. The surface of the

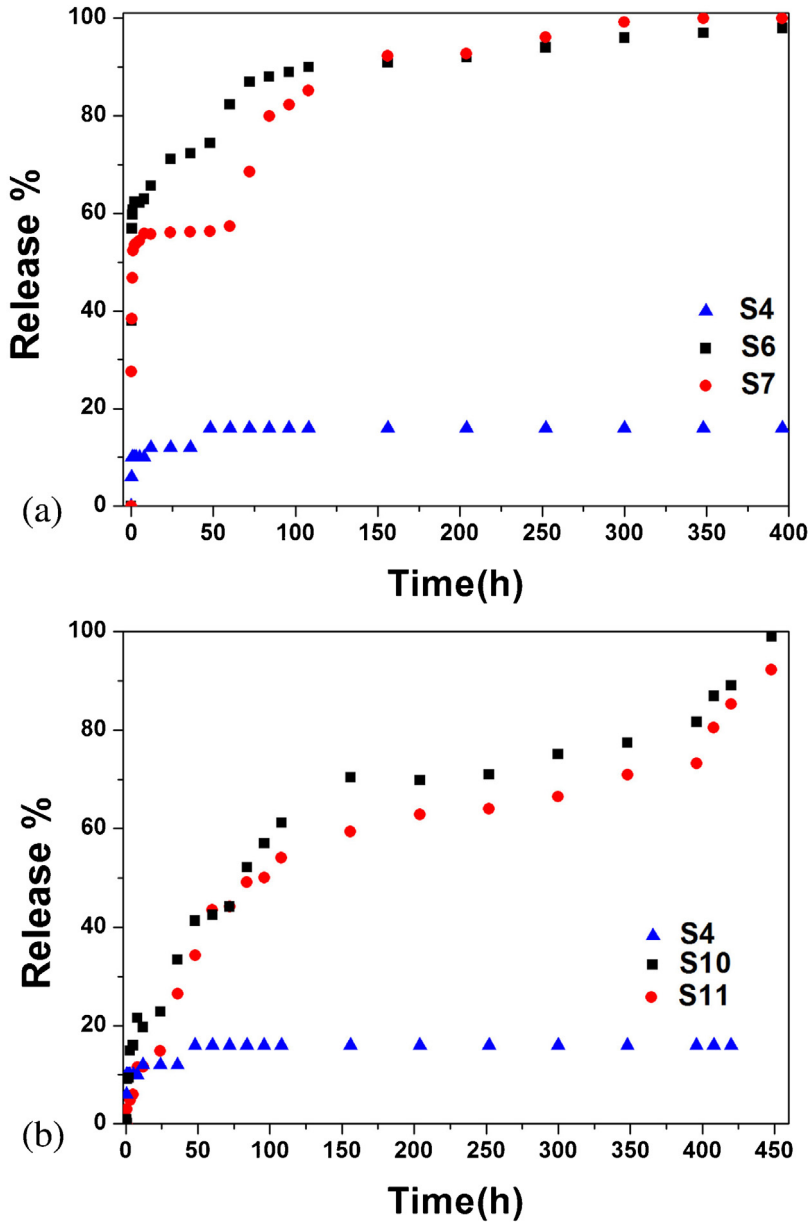

Fig. 7. Drug release pattern for (a) taxol and taxol loaded-MOFs and (b) polymer encapsulated taxol loaded forms.

polymeric matrix for the encapsulated drug loaded samples is rather smooth. However, the cisplatin loaded UiO-67 sample, which was PCL-TPGS encapsulated, seems to have a porous surface.

2.7. Drug release studies

The drug release from the MOFs, before and after being embedded in a biocompatible and biodegradable polymeric matrix is a rather complicated process, where different parameters can affect the release profile. *In vitro* release studies for the cisplatin loaded MOFs before and after encapsulation in the PCL-TPGS polymeric matrix are presented in Fig. 6. The cisplatin drug is a highly hydrophilic active pharmaceutical ingredient (API) and for this reason was fully dissolved within the first 2 h. However, when the drug is loaded in the MOFs, a slower release rate is observed (Fig. 6a). A burst effect can be seen for both UiO-66 and UiO-67 samples, which can be attributed to the drug loading on the surface of the MOFs. After the initial immediate release, a lower rate is observed. The time for complete dissolution of the drug from the MOFs reached 120 h. Comparing the two different cisplatin loaded nano MOFs, in the cisplatin loaded UiO-67 a higher release rate is noticed, probably due to the amorphisation of the sample. However, a sustained release is necessary for anticancer drugs and obviously the neat MOFs may not act as appropriate drug vehicles. Thus, in order to minimize the burst effect, the drug carriers were also microencapsulated in the modified PCL-block-TPGS copolymer (Fig. 6b). *In vitro* release from biodegradable microparticles, as reported in a series of studies, is mainly controlled either by diffusion or erosion and is affected by several factors such as rate of hydrolysis, comonomer ratio, molecular weight and particle size of the prepared microparticles (Burkersroda et al., 2002; Lin et al., 2000; Tamada and Langer, 1993). PCL-TPGS present an enhanced hydrolytic degradation over time (Supporting information Figs. S16 and S17). Surface erosion occurred even after 24 h indicating a possible release mechanism diffusion and erosion phenomenon. From the release curves three main steps can be observed. The microparticles show a burst effect, due to the drug which is mainly located near the surface. During

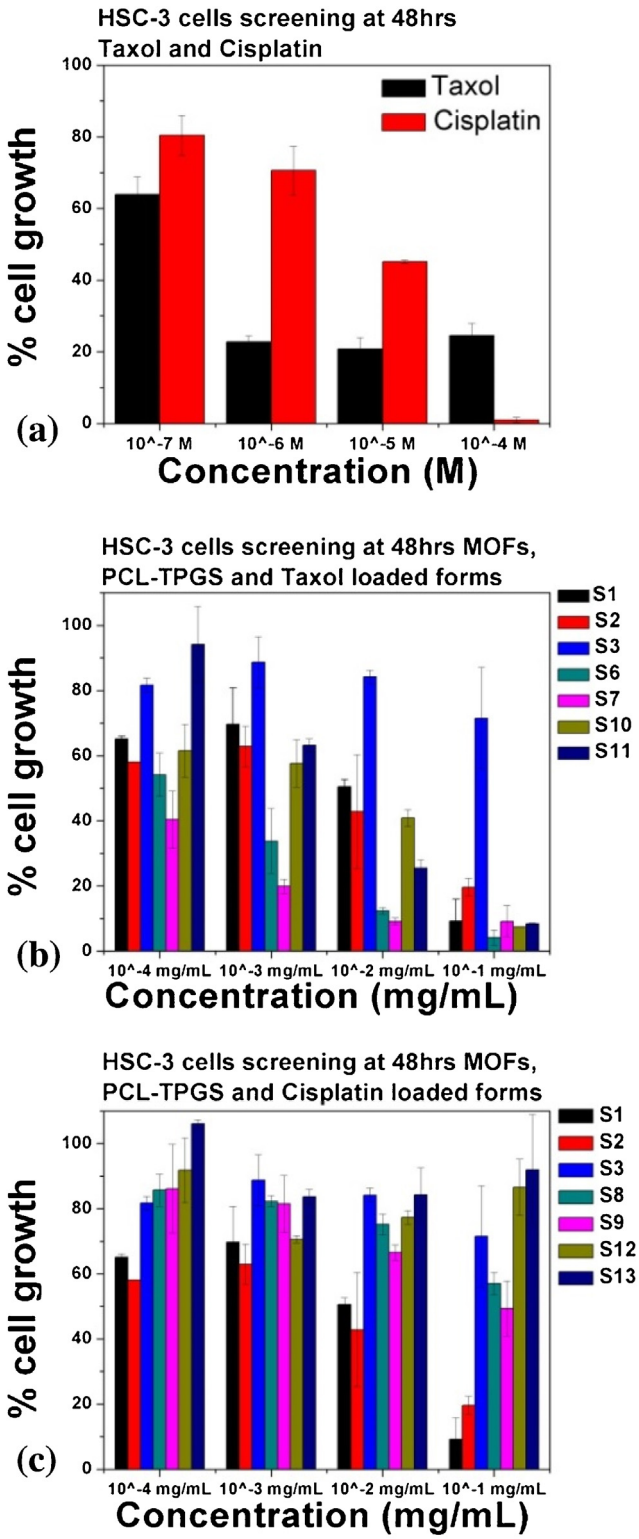

Fig. 8. (a)–(c) Cell growth assessment of HSC-3 cells. Cell viability was assessed after 48 h exposure of the materials in culture at the concentrations indicated, as described under the "Material and Methods section in the Supporting Information". The error bars indicated are mean S.D. (n = 3).

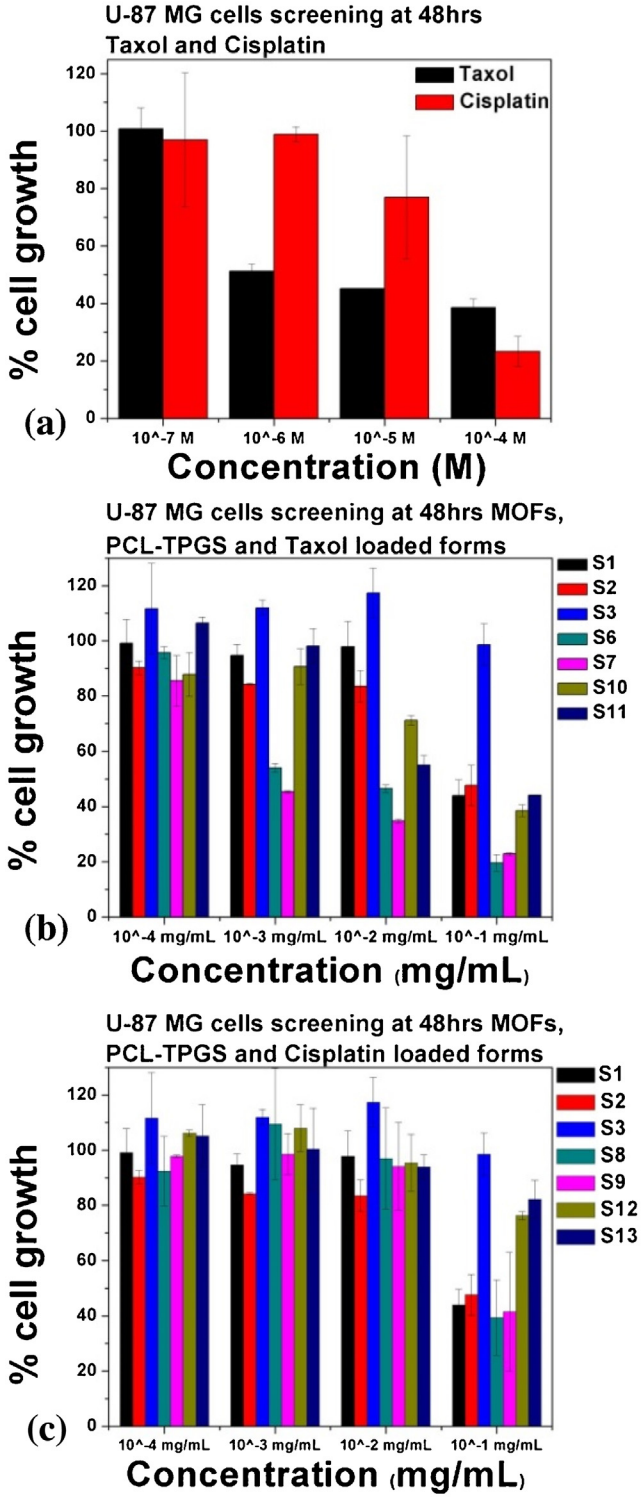

Fig. 9. (a)–(c) Cell growth assessment of U-87 MG cells. Cell viability was assessed after 48 h exposure of the materials in culture at the concentrations indicated, as described under the "Material and Methods section in the Supporting Information". The error bars indicated are mean S.D. (n = 3).

the first 100 h a progressive release is visible achieving a 35% rate for the UiO-67-cisplatin and a lower release rate for the UiO-66-cisplatin sample. At a later stage, a lower increment in the release rate is observed. This slow phase could be produced by diffusion of drugs from the interior of the microparticles and the erosion of the surface. This is in agreement with the hydrolytic studies; the surface did not show a significant variation between 24 and 120 h. Between 132 and 300 h (Ajima et al., 2006; Avgoustakis et al., 2002; Matsumoto et al., 2006), due to the collateral destruction of the polymer microparticles, a much higher increment of the release

rates is observed. At a later stage, the whole amount of the drug is dissolved after 400 h.

In vitro drug release studies were also performed on the taxol loaded MOFs before and after being encapsulated in the polymeric matrix, in simulated body fluid at 37 °C (Fig. 7). A different release mechanism is observed for the taxol samples due to the hydrophobicity of this anticancer agent. Only a small amount of taxol was dissolved after 300 h. However when the same API was absorbed in the MOFs, an enhanced release could be noticed. UiO-67 loaded with taxol presents a lower drug release rate compared to the UiO-66 taxol sample. The increment in UiO-66-taxol dissolution rate is caused by the location of the taxol at the surface as deduced from N2 adsorption measurements. The theoretical measurements also confirmed that taxol cannot diffuse into the crystal of the UiO-66 since there are too few inorganic brick defects (Bernabeu et al., 2014; Huang et al., 2011; Somavarapu et al., 2005). Moreover, the increase of the taxol dissolution rate for both MOFs is due to the fact that the drug was entrapped in an amorphous state, as was revealed by the XRPD measurements. Amorphisation of the drug, in most cases enhances the dissolution rate of poorly soluble drugs, such as taxol (Grobelny et al., 2015). In order to avoid the burst effect and prolong the release rate the taxol loaded MOFs were also microencapsulated in the PCL-TPGS. After the encapsulation of the taxol loaded forms in the PCL-block-TPGS matrix, a controlled release rate is observed. These results are in agreement with our previous work (Filippousi et al., 2013c), as well as other studies, where the hydrolytic degradation which occurs during the dissolution affects the release rate (Fig. S19).

2.8. Cytocompatibility assessment of the materials on the U-87 MG and HSC-3 cancer cell models

Although there are numerous reports describing the synthesis, characterization and applications of the nano MOFs, only a few studies showing the biocompatibility and cytotoxicity behavior in cell models have been reported so far (Ren et al., 2014). Horcajada et al., upon examining the cytotoxicity of 14 nano MOFs using two cell lines (J774 and HeLa), found out that their cytotoxicity capacity strongly depends not only on the MOF composition but also on the cell model (Tamames-Tabar et al., 2014; Ruyra et al., 2015). We demonstrate here the cytocompatibility of the synthesized MOF formulations developed for oral drug delivery which was assessed on U-87 MG (human glioblastoma grade IV; astrocytoma) and HSC-3 (human oral squamous carcinoma) cell models (Kyrodimou et al., 2014; Theodoropoulos et al., 2013). U-87 MG and HSC-3 cells were exposed with increasing concentration (10^{-1} mg/mL–10^{-4} mg/mL) of the MOFs, the drug loaded MOFs as well as their encapsulated forms for 48 h and were compared with the behavior of free-drug exposed cultures (cisplatin or taxol at concentrations of 10^{-4} M–10^{-7} M). Cell viability data demonstrate the concentration-dependent toxicity for all the samples as shown in Figs. 8 and 9. As far as the behavior of the free drugs is concerned in culture, it is seen that taxol exhibits a higher cell growth inhibitory capacity *in vitro* in both HSC-3 and U-87 MG cells compared to cisplatin. Interestingly enough, it has been observed that all materials exhibited a higher cytotoxicity in HSC-3 cells compared to that of U-87 MG cells. Moreover, although the cisplatin is extremely toxic at very high concentrations and especially in HSC-3 cells, when it is loaded in the MOFs and encapsulated in the polymeric matrix its cytotoxicity is significantly improved. Similar results were also found for the taxol and for the neat MOFs. It is important to note that the polymer coated drug-loaded nano MOFs are not cytotoxic under the same cell culture conditions, as shown by the cellular viability data, indicating that the *in vitro* biocompatibility behavior of the polymer encapsulated nanomaterials is very promising.

3. Conclusions

Nanoscale metal organic frameworks UiO-66 and UiO-67 with uniform particle size were synthesized and successfully used as drug delivery carriers. The surfaces of the Zr-based nano MOFs were further engineered by microencapsulated them with a biocompatible and biodegradable polymeric matrix in order to enhance their water dispersibility and biocompatibility. Even though the organic systems have the advantage of providing biocompatibility, the nano MOFs were used in order to deliver the drugs in a controlled manner due to their porous and crystalline nature. The *in vitro* drug release measurements in the case of the cisplatin loaded forms, before and after the encapsulation, revealed a sustained release rate. For the taxol loaded forms a high dissolution rate was observed due to the amorphisation of the drug. Importantly, the encapsulation of the drug loaded MOFs inside the biocompatible and biodegradable polymeric matrix enhances the sustained release and decreases the burst effect. The cytotoxicity of all the studied samples was evaluated by the MTT assay using two cell lines (U-87 MG and HSC-3), indicating low toxicity for the polymer coated forms, even in high concentrations and in both cell lines. These studies demonstrate that this type of materials display a huge application potential in the field of drug delivery, due to both the porous structure of the nano MOFs and the biocompatibility of the polymer drug loaded forms.

Acknowledgements

This work is performed within the framework of the IAP-P7/05. S.T. Gratefully acknowledges the Fund for Scientific Research Flanders (FWO). K.L. acknowledges the financial support from the Ghent University BOF postdoctoral grant 01P06813T and UGent GOA Grant 01G00710.These and the Reference headings are in bold but have no numbers. Text below continues as normal.

Appendix A. Supplementary data

Supplementary data associated with this article can be found, in the online version, at http://dx.doi.org/10.1016/j.ijpharm.2016.05.048.

Materials and methods, detailed synthetic procedures, characterization for all the studied samples and figures (Fig. S1–S20).

References

Ajima, K., Yudasaka, M., Maigné, A., Miyawaki, J., Iijima, S., 2006. Effect of functional groups at hole edges on cisplatin release from inside single-wall carbon nanohorns. J. Phys. Chem. B 110, 5773–5778. doi:http://dx.doi.org/10.1021/jp056813x.

Avgoustakis, K., Beletsi, A., Panagi, Z., Klepetsanis, P., Karydas, A.G., Ithakissios, D.S., 2002. PLGA-mPEG nanoparticles of cisplatin: *in vitro* nanoparticle degradation, *in vitro* drug release and in vivo drug residence in blood properties. J. Control. Release 79, 123–135. doi:http://dx.doi.org/10.1016/S0168-3659(01)00530-2.

Bernabeu, E., Helguera, G., Legaspi, M.J., Gonzalez, L., Hocht, C., Taira, C., Chiappetta, D.A., 2014. Paclitaxel-loaded PCL-TPGS nanoparticles: *in vitro* and in vivo performance compared with Abraxane®. Colloids Surf. B: Biointerfaces 113, 43–50. doi:http://dx.doi.org/10.1016/j.colsurfb.2013.07.036.

Burkersroda, F., von Schedl, L., Göpferich, A., 2002. Why degradable polymers undergo surface erosion or bulk erosion. Biomaterials 23, 4221–4231. doi:http://dx.doi.org/10.1016/S0142-9612(02)00170-9.

Cavka, J.H., Jakobsen, S., Olsbye, U., Guillou, N., Lamberti, C., Bordiga, S., Lillerud, K.P., 2008. A new zirconium inorganic building brick forming metal organic frameworks with exceptional stability. J. Am. Chem. Soc. 130, 13850–13851. doi:http://dx.doi.org/10.1021/ja8057953.

Ciardelli, G., Chiono, V., Vozzi, G., Pracella, M., Ahluwalia, A., Barbani, N., Cristallini, C., Giusti, P., 2005. Blends of poly-(ε-caprolactone) and polysaccharides in tissue engineering applications. Biomacromolecules 6, 1961–1976. doi:http://dx.doi.org/10.1021/bm0500805.

Cliffe, M.J., Wan, W., Zou, X., Chater, P.A., Kleppe, A.K., Tucker, M.G., Wilhelm, H., Funnell, N.P., Coudert, F.-X., Goodwin, A.L., 2014. Correlated defect nanoregions in a metal-organic framework. Nat. Commun. 5, 4176. doi:http://dx.doi.org/10.1038/ncomms5176.

Della Rocca, J., Liu, D., Lin, W., 2013. Nanoscale metal-organic frameworks for biomedical imaging and drug delivery. Acc. Chem. Res. 44, 957–968. doi:http://dx.doi.org/10.1021/ar200028a.
Férey, G., 2008. Hybrid porous solids: past, present, future. Chem. Soc. Rev. 37, 191–214. doi:http://dx.doi.org/10.1039/b618320b.
Farrusseng, D., Aguado, S., Pinel, C., 2009. Metal-organic frameworks: opportunities for catalysis. Angew. Chem. Int. Ed. 48, 7502–7513. doi:http://dx.doi.org/10.1002/anie.200806063.
Filippousi, M., Altantzis, T., Stefanou, G., Betsiou, M., Bikiaris, D.N., Angelakeris, M., Pavlidou, E., Zamboulis, D., Van Tendeloo, G., 2013a. Polyhedral iron oxide core–shell nanoparticles in a biodegradable polymeric matrix: preparation, characterization and application in magnetic particle hyperthermia and drug delivery. RSC Adv. 3, 24367. doi:http://dx.doi.org/10.1039/c3ra43747g.
Filippousi, M., Papadimitriou, S.A., Bikiaris, D.N., Pavlidou, E., Angelakeris, M., Zamboulis, D., Tian, H., Van Tendeloo, G., 2013b. Novel core–shell magnetic nanoparticles for taxol encapsulation in biodegradable and biocompatible block copolymers: preparation, characterization and release properties. Int. J. Pharm. 448, 221–230. doi:http://dx.doi.org/10.1016/j.ijpharm.2013.03.025.
Filippousi, M., Altantzis, T., Stefanou, G., Betsiou, M., Bikiaris, D.N., Angelakeris, M., Pavlidou, E., Zamboulis, D., Van Tendeloo, G., 2013c. Polyhedral iron oxide core–shell nanoparticles in a biodegradable polymeric matrix: preparation, characterization and application in magnetic particle hyperthermia and drug delivery. RSC Adv. 3 (46), 24367.
Filippousi, M., Siafaka, P.I., Amanatiadou, E.P., Nanaki, S.G., Neratzaki, M., Bikiaris, D. N., Vizirianakis, I.S., Van Tendeloo, G., 2015. Modified chitosan coated mesoporous strontium hydroxyapatite nanorods as drug carriers. J. Mater. Chem. B doi:http://dx.doi.org/10.1039/C5TB00827A.
Grobelny, P., Kazakevich, I., Zhang, D., Bogner, R., 2015. Amorphization of itraconazole by inorganic pharmaceutical excipients: comparison of excipients and processing methods. Pharm. Dev. Technol. 20, 118–127. doi:http://dx.doi.org/10.3109/10837450.2014.959181.
Horcajada, P., Serre, C., Vallet-Regí, M., Sebban, M., Taulelle, F., Férey, G., 2006. Metal-organic frameworks as efficient materials for drug delivery. Angew. Chem. Int. Ed. 45, 5974–5978. doi:http://dx.doi.org/10.1002/anie.200601878.
Horcajada, P., Serre, C., Maurin, G., Ramsahye, N.A., Balas, F., Vallet-Regí, M., Sebban, M., Taulelle, F., Férey, G., 2008. Flexible porous metal-organic frameworks for a controlled drug delivery. J. Am. Chem. Soc. 130 (21), 6774–6780. doi:http://dx.doi.org/10.1021/ja710973k.
Horcajada, P., Chalati, T., Serre, C., Gillet, B., Sebrie, C., Baati, T., Eubank, J.F., Heurtaux, D., Clayette, P., Kreuz, C., Chang, J.-S., Hwang, Y.K., Marsaud, V., Bories, P.-N., Cynober, L., Gil, S., Férey, G., Couvreur, P., Gref, R., 2010. Porous metal-organic-framework nanoscale carriers as a potential platform for drug delivery and imaging. Nat. Mater. 9, 172–178. doi:http://dx.doi.org/10.1038/nmat2608.
Huang, L., Chen, H., Zheng, Y., Song, X., Liu, R., Liu, K., Zeng, X., Mei, L., 2011. Nanoformulation of d-α-tocopheryl polyethylene glycol 1000 succinate-b-poly (ε-caprolactone-ran-glycolide) diblock copolymer for breast cancer therapy. Integr. Biol. doi:http://dx.doi.org/10.1039/c1ib00026h.
Huxford, R.C., Della Rocca, J., Lin, W., 2010. Metal-organic frameworks as potential drug carriers. Curr. Opin. Chem. Biol. 14, 262–268. doi:http://dx.doi.org/10.1016/j.cbpa.2009.12.012.
Jain, V., Jain, B., Tiwari, P., Saini, J., Jain, U.K., Pandey, R.S., Kumar, M., Katare, O.P., Chandra, R., Madan, J., 2013. Nanosolvated microtubule-modulating chemotherapeutics. Anticancer. Drugs 24, 327–336. doi:http://dx.doi.org/10.1097/CAD.0b013e32835ec414.
Jiang, L., Li, X., Liu, L., Zhang, Q., 2013. Thiolated chitosan-modified PLA-PCL-TPGS nanoparticles for oral chemotherapy of lung cancer. Nanoscale Res. Lett. 8, 66. doi:http://dx.doi.org/10.1186/1556-276X-8-66.
Keskin, S., Kızılel, S., 2011. Biomedical applications of metal organic frameworks. Ind. Eng. Chem. Res. doi:http://dx.doi.org/10.1021/ie101312k.
Kyrodimou, M., Andreadis, D., Drougou, A., Amanatiadou, E.P., Angelis, L., Barbatis, C., Epivatianos, A., Vizirianakis, I.S., 2014. Desmoglein-3/γ-catenin and E-cadherin/β-catenin differential expression in oral leukoplakia and squamous cell carcinoma. Clin. Oral Investig. 18, 199–210. doi:http://dx.doi.org/10.1007/s00784-013-0937-z.
Lin, S.-Y., Chen, K.-S., Teng, H.-H., Li, M.-J., 2000. In vitro degradation and dissolution behaviours of microspheres prepared by three low molecular weight polyesters. J. Microencapsul. 17, 577–586. doi:http://dx.doi.org/10.1080/026520400417630.
Ma, Y., Huang, L., Song, C., Zeng, X., Liu, G., Mei, L., 2010. Nanoparticle formulation of poly(ε-caprolactone-co-lactide)-D-α-tocopheryl polyethylene glycol 1000 succinate random copolymer for cervical cancer treatment. Polymer (Guildf). 51, 5952–5959. doi:http://dx.doi.org/10.1016/j.polymer.2010.10.029.
Marquette, S., Peerboom, C., Yates, A., Denis, L., Langer, I., Amighi, K., Goole, J., 2014. Stability study of full-length antibody (anti-TNF alpha) loaded PLGA microspheres. Int. J. Pharm. 470, 41–50. doi:http://dx.doi.org/10.1016/j.ijpharm.2014.04.063.
Mastropaolo, D., Camerman, A., Luo, Y., Brayer, G.D., Camerman, N., 1995. Crystal and molecular structure of paclitaxel (taxol). Proc. Natl. Acad. Sci. 92, 6920–6924. doi:http://dx.doi.org/10.1073/pnas.92.15.6920.
Matsumoto, A., Matsukawa, Y., Horikiri, Y., Suzuki, T., 2006. Rupture and drug release characteristics of multi-reservoir type microspheres with poly(DL-lactide-co-glycolide) and poly(DL-lactide). Int. J. Pharm. 327, 110–116. doi:http://dx.doi.org/10.1016/j.ijpharm.2006.07.055.
Mei, L., Zhang, Z., Zhao, L., Huang, L., Yang, X.L., Tang, J., Feng, S.S., 2013. Pharmaceutical nanotechnology for oral delivery of anticancer drugs. Adv. Drug Deliv. Rev. 65, 880–890. doi:http://dx.doi.org/10.1016/j.addr.2012.11.005.
Meledina, M., Turner, S., Filippousi, M., Leus, K., Lobato, I., Ramachandran, R.K., Dendooven, J., Detavernier, C., Van Der Voort, P., Van Tendeloo, G., 2016. Direct imaging of ALD deposited Pt nanoclusters inside the giant pores of MIL-101. Part. Part. Syst. Charact. 1–6. doi:http://dx.doi.org/10.1002/ppsc.201500252.
Milburn, G.H.W., Truter, M.R., 1966. The crystal structures of cis- and trans-dichlorodiammineplatinum(II). J. Chem. Soc. A: Inorg. Phys. Theor. 1609 doi:http://dx.doi.org/10.1039/j19660001609.
Ravon, U., Domine, M., Gaudillère, C., Desmartin-Chomel, A., Farrusseng, D., 2008. MOF-5 as acid catalyst with shape selectivity properties. Stud. Surf. Sci. Catal. 467–470. doi:http://dx.doi.org/10.1016/S0167-2991(08)80242-X.
Ravon, U., Savonnet, M., Aguado, S., Domine, M.E., Janneau, E., Farrusseng, D., 2010. Engineering of coordination polymers for shape selective alkylation of large aromatics and the role of defects. Microporous Mesoporous Mater. 129, 319–329. doi:http://dx.doi.org/10.1016/j.micromeso.2009.06.008.
Ren, F., Jing, Q., Cui, J., Shen, Y., 2009. Synthesis and characterization of D-α-tocopheryl polyethylene glycol 1000 succinate-block-poly (ε-caprolactone) copolymer used as carriers for microparticles. J. Dispers. Sci. Technol. doi:http://dx.doi.org/10.1080/01932690802701507.
Ren, F., Yang, B., Cai, J., Jiang, Y., Xu, J., Wang, S., 2014. Toxic effect of zinc nanoscale metal-organic frameworks on rat pheochromocytoma (PC12) cells *in vitro*. J. Hazard. Mater. 271, 283–291. doi:http://dx.doi.org/10.1016/j.jhazmat.2014.02.026.
Ruyra, À., Yazdi, A., Espín, J., Carné-Sánchez, A., Roher, N., Lorenzo, J., Imaz, I., Maspoch, D., 2015. Synthesis, culture medium stability, and in vitro and In vivo zebrafish embryo toxicity of metal-organic framework nanoparticles. Chem. A: Eur. J. 21, 2508–2518. doi:http://dx.doi.org/10.1002/chem.201405380.
Sinha, V.R., Trehan, A., 2003. Biodegradable microspheres for protein delivery. J. Control. Release 90, 261–280. doi:http://dx.doi.org/10.1016/S0168-3659(03)00194-9.
Sokol, R.J., Butler-Simon, N., Conner, C., Heubi, J.E., Sinatra, F.R., Suchy, F.J., Heyman, M.B., Perrault, J., Rothbaum, R.J., Levy, J., 1993. Multicenter trial of d-alpha-tocopheryl polyethylene glycol 1000 succinate for treatment of vitamin E deficiency in children with chronic cholestasis. Gastroenterology 104 (6), 1727–1735 (PMID:8500733).
Somavarapu, S., Pandit, S., Gradassi, G., Bandera, M., Ravichandran, E., Alpar, O.H., 2005. Effect of Vitamin E TPGS on immune response to nasally delivered diphtheria toxoid loaded poly(caprolactone) microparticles. Int. J. Pharm. 344–347. doi:http://dx.doi.org/10.1016/j.ijpharm.2005.03.029.
Tamada, J.A., Langer, R., 1993. Erosion kinetics of hydrolytically degradable polymers. Proc. Natl. Acad. Sci. 90, 552–556. doi:http://dx.doi.org/10.1073/pnas.90.2.552.
Tamames-Tabar, C., Cunha, D., Imbuluzqueta, E., Ragon, F., Serre, C., Blanco-Prieto, M. J., Horcajada, P., 2014. Cytotoxicity of nanoscaled metal-organic frameworks. J. Mater. Chem. B 2, 262–271. doi:http://dx.doi.org/10.1039/c3tb20832j.
Taylor-Pashow, K.M.L., Della Rocca, J., Xie, Z., Tran, S., Lin, W., 2009. Postsynthetic modifications of iron-carboxylate nanoscale metal-organic frameworks for imaging and drug delivery. J. Am. Chem. Soc. 131, 14261–14263. doi:http://dx.doi.org/10.1021/ja906198y.
Theodoropoulos, D., Rova, A., Smith, J.R., Barbu, E., Calabrese, G., Vizirianakis, I.S., Tsibouklis, J., Fatouros, D.G., 2013. Towards boron neutron capture therapy: the formulation and preliminary *in vitro* evaluation of liposomal vehicles for the therapeutic delivery of the dequalinium salt of bis-nido-carborane. Bioorg. Med. Chem. Lett. 23, 6161–6166. doi:http://dx.doi.org/10.1016/j.bmcl.2013.09.003.
Trewyn, B.G., Giri, S., Slowing, I.I., Lin, V.S.-Y., 2007. Mesoporous silica nanoparticle based controlled release, drug delivery, and biosensor systems. Chem. Commun. (Camb.) 3236–3245. doi:http://dx.doi.org/10.1039/b701744h.
Vandichel, M., Hajek, J., Vermoortele, F., Waroquier, M., De Vos, D.E., Van Speybroeck, V., 2015. Active site engineering in UiO-66 type metal-organic frameworks by intentional creation of defects: a theoretical rationalization. CrystEngComm 17, 395–406. doi:http://dx.doi.org/10.1039/C4CE01672F.
Vermoortele, F., Bueken, B., Le Bars, G., Van De Voorde, B., Vandichel, M., Houthoofd, K., Vimont, A., Daturi, M., Waroquier, M., Van Speybroeck, V., Kirschhock, C., De Vos, D.E., 2013. Synthesis modulation as a tool to increase the catalytic activity of metal-organic frameworks: The unique case of UiO-66(Zr). J. Am. Chem. Soc. 135, 11465–11468. doi:http://dx.doi.org/10.1021/ja405078u.
Yang, Y., Chung, T., Ngee Ping, N., 2001. Morphology, drug distribution, and *in vitro* release pro les of biodegradable polymeric microspheres containing protein fabricated by double-emulsion solvent extraction/evaporation method. Biomaterials 22, 231–241.
Zhao, M., Deng, C., Zhang, X., 2014. The design and synthesis of a hydrophilic core-shell-shell structured magnetic metal-organic framework as a novel immobilized metal ion affinity platform for phosphoproteome research. Chem. Commun. (Camb.) 50, 6228–6231. doi:http://dx.doi.org/10.1039/c4cc01038h.
Zhu, L., Zhang, D., Xue, M., Li, H., Qiu, S., 2013. Direct observations of the MOF (UiO-66) structure by transmission electron microscopy. CrystEngComm 15, 9356. doi:http://dx.doi.org/10.1039/c3ce41122b.
Zhu, X., Gu, J., Wang, Y., Li, B., Li, Y., Zhao, W., Shi, J., 2014. Inherent anchorages in UiO-66 nanoparticles for efficient capture of alendronate and its mediated release. Chem. Commun. (Camb.) 8779–8782. doi:http://dx.doi.org/10.1039/c4cc02570a.
Zhuang, J., Kuo, C.H., Chou, L.Y., Liu, D.Y., Weerapana, E., Tsung, C.K., 2014. Optimized metal-organic-framework nanospheres for drug delivery: evaluation of small-molecule encapsulation. ACS Nano 8, 2812–2819. doi:http://dx.doi.org/10.1021/nn406590q.